Science Capabilities of the VERITAS array of 10m Imaging Atmospheric Cherenkov gamma-ray detectors

D. Kieda[a**], S.D. Biller[b], P. Boyle[c], I.H. Bond[d], S. M. Bradbury[d], J. H. Buckley[e],D.A. Carter-Lewis[f], S. Criswell[g], W. Cui[h], P. Dowkontt[e], C. Duke[i], A. Falcone[h], D.J. Fegan[j], S.J. Fegan[g,k]; J.P. Finley[h], L. Fortson[l], J.A. Gaidos[h], S. Gammell[j], K. Gibbs[g], J. Hall[s]; A.M. Hillas[d], J. Holder[d], D. Horan[g], M. Kertzman[m], J. Knapp[d], F. Krennrich[f], S. LeBohec[f], J. Lloyd-Evans[d]; P. Moriarity[n], D. Müller[c], P. Ogden[d], R. Ong[o], D. Petry[f], J. Quinn[j], P.T. Reynolds[p], H.J. Rose[d] ,M. Schroedter[g,k], J. Smith[a], G.H. Sembrowski[h], S.P. Swordy[c], V. V. Vassiliev[a], S.P. Wakely[c], G.Walker[a] and T.C. Weekes[g]

[a]University of Utah; [b]Oxford University(UK); [c]University of Chicago; [d]University of Leeds (UK); [e]Washington University St. Louis; [f]Iowa State University; [g]Whipple Observatory, Harvard Smithsonian CfA; [h]Purdue University; [i]Grinnell College; [j]National University of Ireland, Dublin; [k]University of Arizona; [l]Adler Planetarium (Chicago); [m]DePauw University; [n]Galway-Mayo Institute of Technology(Ireland); [o]University of California (Los Angeles); [p]Cork Institute of Technology (Ireland)

ABSTRACT

The Very Energetic Radiation Imaging Telescope Array System (VERITAS) is an array of seven 10m aperture telescopes used for gamma-ray astronomy in the 50 GeV to 50 TeV (1 TeV= 10^{12} electron Volt) energy range. The gamma rays are detected by measuring the optical Cherenkov light emitted by the cascade of electromagnetic particles that is generated by interactions of the high energy gamma-ray with the Earth's Atmosphere. This paper describes the science goals of the VERITAS array, a description of the array, and expected performance of the instrument.

Keywords: VERITAS; gamma-ray Astronomy; gamma-ray telescopes; Atmospheric Cherenkov radiation, Pulsars; AGN; Supernova remnants; Galactic Plane; Neutralinos; Cosmic rays; Fundamental Physics

1. Science Goals

The field of ground-based gamma-ray astronomy has been revolutionized by the power of the atmospheric Cherenkov imaging technique for the discovery and study of discrete sources of high energy radiation. This technique was largely developed by the Whipple Observatory Gamma-Ray Collaboration[1,2]. Although less than 1% of the sky has been surveyed by the imaging technique at 300 GeV, fifteen sources have now been reported (eight with high significance) by ground-based groups using the imaging technique: three pulsar-powered nebulae, eight BL-Lacertae-type active galactic nuclei (AGN), three shell-type supernova remnants, and one X-ray binary system[3]. These measurements have advanced our understanding of the origin of cosmic rays, the nature of AGN jets, the density of the astrophysical background infrared radiation (IR), and the magnetic fields within supernova remnants. The VERITAS array[4], it its substantially improved resolution and sensitivity, will open up new opportunities for detailed studies of existing TeV gamma-ray emitters as well as open up the possibility for discovery of new sources and new fundamental physics phenomena.

1.1. Active Galactic Nuclei (AGN)

AGN are galaxies with resolved central nucleus that outshines the rest of the galaxy and for which the emission is often dominated by nonthermal processes. Their emission is widely believed to be powered by accretion onto a supermassive black hole. Currently, no model for the production of gamma-rays in AGN is generally accepted. The two most popular models of gamma-production are those in which high energy electrons produce gamma-rays by inverse Compton scattering off low energy photons, and those in which high energy protons produce pions through nuclear interactions, which subsequently decay into high energy gamma-rays(Figure 1).

** Presenting Author

Discoveries and Research Prospects from 6- to 10-Meter-Class Telescopes II, Puragra Guhathakurta, Editor, Proceedings of SPIE Vol. 4834 (2003) © 2003 SPIE · 0277-786X/03/$15.00

VHE observations of blazars have proven to be critical for understanding of the physics operating in this class of AGN. Whipple observations of the BL Lacertae (BL Lac) objects Markarian 421 (Mrk 421) and Mrk 501 have revealed extremely variable VHE emission[5,6] (Figure 2). Variability on a 15 minute time scale[6] observed in Mkn 421 implies a compact γ-ray emitting region of 10^{-4} parsec, only an order of magnitude larger than the event horizon radius for a 10^8 solar mass black hole. Correlations observed between X-rays and TeV gamma-rays[7,8,9] are most easily explained as emission produced by the same population of energetic electrons. The tendency of VHE telescopes to detect X-ray selected BL Lac objects and of EGRET to detect radio selected BL Lac objects and flat-spectrum radio quasars also supports a prominent role of electrons in the AGN jets. However, models that produce γ-rays primarily through proton interactions[10] can also explain most of the observations to date. The Whipple and EGRET data have also led to reformulation of blazar unification models based on intrinsic source luminosity rather than solely on the effects of orientation differences[11,12,13].

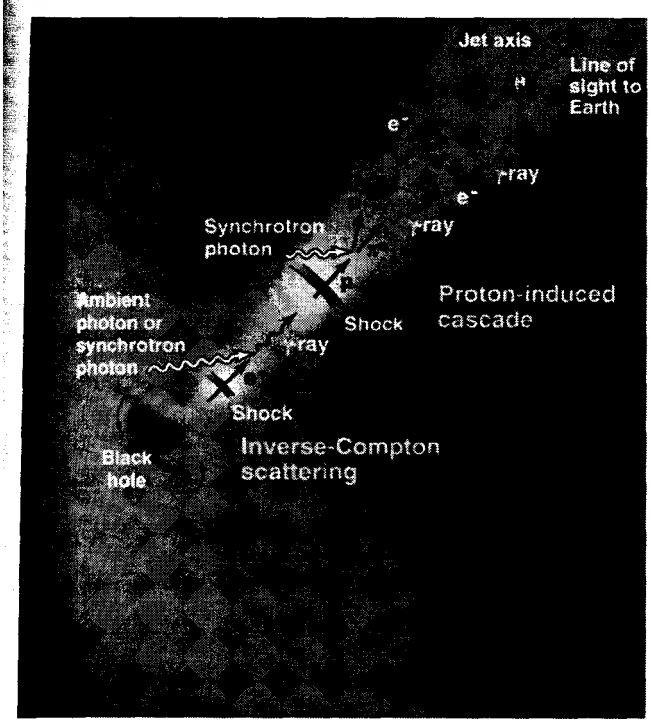

Figure 1: Artist's conception of the nucleus of an active galaxy[14]. Two possible scenarios for the production of gamma-rays in a relativistic jet are illustrated.

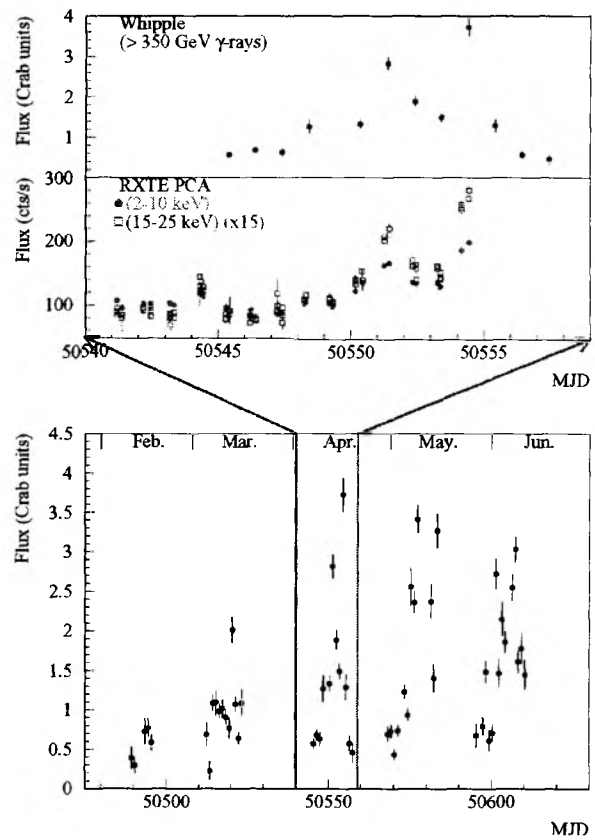

Figure 2: Upper panel: Observations of Mkn501 in TeV gamma-rays (top) and X-rays(bottom) taken during 1997 April 2-20 (April 2 corresponds to MJD 50540)[5]. Lower Panel: Average daily gamma-ray rates observed with Whipple for Mkn 501 in 1997.

1.2. *Shell-type Supernova Remnants and Cosmic Rays*

Supernova remnants (SNRs) are widely believed to provide sources of nuclear cosmic rays up to energies of approximately Z × 100 TeV, where Z is the nuclear charge of the particle[15]. This hypothesis is supported by the observed supernova energy output and occurrence rate, which is sufficient to provide enough energy to maintain the observed Galactic cosmic ray density. The existence of energetic electrons in SNR is well established from observations of

synchrotron emission at radio and X-ray energies[16], and recently emission of TeV gamma-rays from SNR have been observed[3,17] Similar to TeV emission in AGN jets, SNR gamma-rays may be emitted through inverse Compton scattering of energetic electrons off low energy photons, or may be produced through the decay of pions created by nuclear interactions of accelerated nuclei with the surrounding SNR ejecta[18] (Figure 3). From this Figure, it is likely that SNR emission from both types of processes may be occurring. Resolving the individual components of the different production mechanisms may only be possible through accurate measurements of gamma-ray flux over a wide range of energies. Next generation gamma-ray observatories like VERITAS and GLAST may provide sufficient energy coverage and energy resolution to untangle these two components.

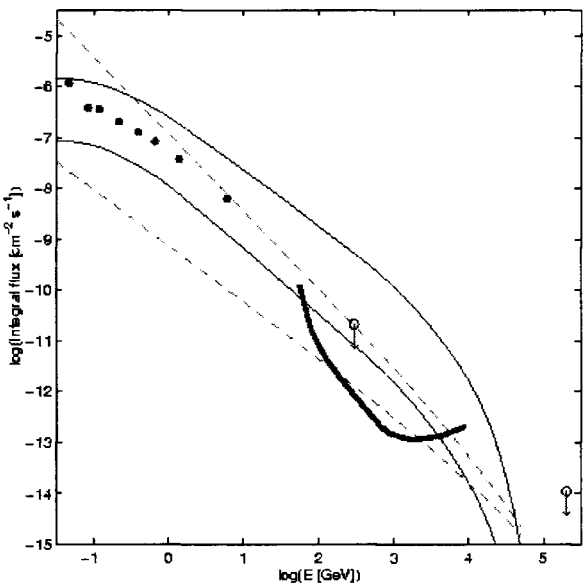

Figure 3: Predicted gamma-ray spectra in shell-type SNR IC443. The region between the solid lines depicts the spectra from hadronic interactions for a range of model parameters[18]. The region between the dashed lines is the predicted inverse-Compton spectra for magnetic field B between 20 μGauss and 50 μGauss and the range of flux normalizations and electron spectra allowed by the X-ray observations. EGRET data points (filled circles) and current upper limits (open circles) from Whipple and Cygnus air shower array are shown. The sensitivity of VERITAS for a 50 hour observation of this object is indicated by the thick curve.

1.3. Compact Galactic Objects

Several pulsar-powered nebulae (Crab nebula[2], PSR1706-44[19], and the Vela Pulsar[20]) have been observed at TeV energies. A crucial step towards understanding the production mechanism of these gamma-rays is to accurately determine the energy spectrum of this emission. Combined with observations of synchrotron emission spectrum, TeV measurements have been used to derive direct measurements of the nebular magnetic field.

Other potential galactic sources observed at lower gamma ray energies include gamma-ray pulsars, X-ray binaries, galactic plane, and the unidentified EGRET sources[3]. Although not detected with present generation gamma ray observatories, higher sensitivity observatories like VERITAS may attain sufficient sensitivity to detect TeV emission from some of these unusual astrophysical objects.

1.4. Background Infrared Radiation

In traversing intergalactic distances, TeV gamma-rays can be absorbed by photon-photon pair production on background infrared photon fields[21]. Intergalactic IR photons arise from galaxy formation, with the spectrum and density of IR radiation yielding information about the epoch and evolution of the formation process. Exotic mechanisms, such as decay of massive neutrinos or presence of various dark matter constituents may also contribute to the IR background. Measurements of TeV gamma ray spectra from distant source can provide indirect investigation of the extragalactic IR field through the distortion induced in the gamma-ray spectrum due to pair production[22,23,24]. At some wavelengths these limits are an order of magnitude better than upper limits produced by the DIRBE/COBE satellite[25] (Figure 4), and already have improved limits on the lifetime/branching ratio for radiative decay of heavy (~0.05 eV) neutrinos by up to 2 orders of magnitude[24]. With its additional sensitivity to view more distant sources, VERITAS can substantially improve these limits, and potentially detect the effects of the IR field.

1.5. Particle Physics and Fundamental physics

The higher sensitivity and larger detection area of the VERITAS telescope opens up the possibility for detection of a number of new phenomena which would have significant impact on our understanding of particle physics and fundamental physics. Potential science investigations include:

- Searching for prompt TeV emission from Gamma Ray Bursts as a method for distinguishing between various origin models of GRBs [26].
- Search for gamma-ray emission form evaporation of low mass black holes created in the early universe via gravitational collapse of inhomogeneities[27,28,29,30].
- Search for time delay effects in bursts of gamma rays due to effects of quantum gravity[31,32,33].
- Search for radiative annihilation of potential supersymmetric dark matter candidates such as the neutralino in the Galactic center[34,35].
- High resolution measurements of charged cosmic ray composition[36], and searches for heavy nuclei and unusual charge states such as quark matter[37,38] and relativistic magnetic monopoles[39] in the cosmic ray flux.

2. Imaging Technique for Atmospheric Cherenkov Radiation

A high energy gamma-ray impinging on the Earth's atmosphere makes a highly elongated shower of relativistic electrons and positrons, generating an intense beam of optical Cherenkov light which is highly collimated from the direction of origin of the primary gamma-ray. Optical images of the Cherenkov light are recorded using an array of photomultiplier tubes (PMTs) located in the focal plane of a large optical reflector (Figure 5). Ground-Based VHE gamma-ray telescopes have an inherent advantage over satellite-borne telescopes due to their very large detection areas (> 40,000 m^2 compared with < 1 m^2). However, unlike satellite instruments, atmospheric Cherenkov telescopes must use additional techniques to reject the large background of charged cosmic rays that can overwhelm the weak gamma-ray signal.

The atmospheric Cherenkov imaging technique was proposed 25 years ago[40] to exploit systematic differences between Cherenkov images generated by gamma-rays and by charged cosmic rays. Gamma-ray induced Cherenkov images are the result of purely electromagnetic processes, and therefore tend to have narrower images (compared to Cherenkov images generated by charged cosmic rays). Cherenkov images from a point source of gamma-rays observed with the source on axis also have a preferred orientation: these Cherenkov images point back to a single point of origin at the center of the field of view. Background cosmic rays come from all directions and therefore have no preferred orientation. The power of this technique was first demonstrated by detection of the Crab nebular using the Whipple 10m reflector with a relatively coarse pixel camera[1,2]; background was rejected with 99.7% efficiency, and source location was found to be accurate to within 0.05°.

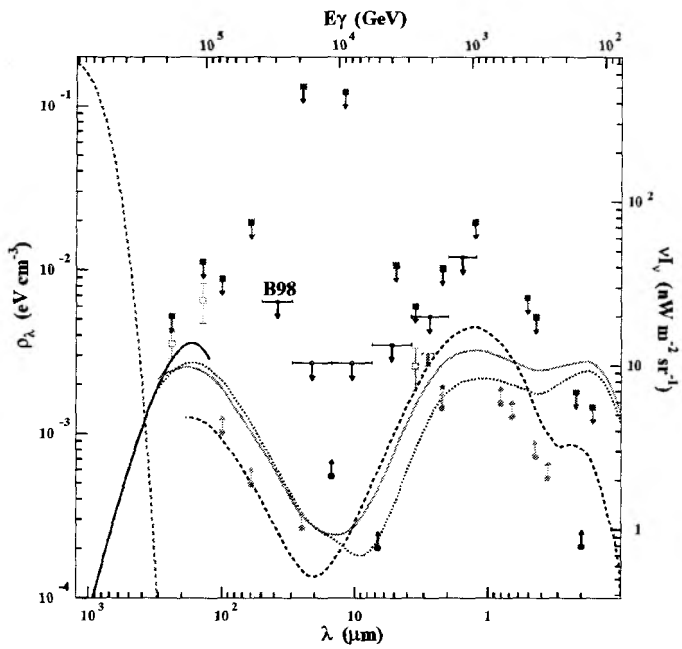

Figure 4: The diffuse intergalactic infrared background. E_γ is the energy at which the pair-production cross-section peaks for head-on collisions with photons of wavelength λ. Upper limits derived from gamma-ray spectra are shown as horizontal bars with arrows[25], marked as B98. The points and the slid curve represent experimental limits or detections. The dashed line on the left is the 2.7 K cosmic microwave background and the three dashed curves are models of the IR background.

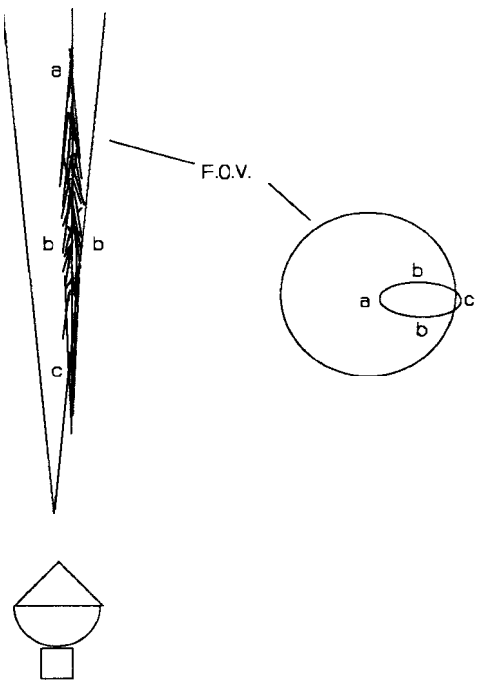

Figure 5: The atmospheric Cherenkov imaging technique. The cone of acceptance of the camera intercepts the core of the air shower. The elliptical contour of a typical Cherenkov light image as seen in the focal plane of the Whipple Observatory camera (diameter 3.5°) is shown on the right. Images of gamma-ray showers coming from a source in the center of the field of view are narrow and point towards the center. Images from background cosmic rays are broader and

Following the discovery of the Crab Nebula as a steady source of TeV gamma-rays, substantial improvements in gamma-ray sensitivity have been realized through the use of finer camera pixelization and optimized analysis techniques[41], arrays of Cherenkov Imaging telescopes[42,43] and fast readout electronics[44]. Finer pixelization and fast readout electronics serve to minimize night sky background contributions to pixel information, and also help to determine direction of shower travel within the shower image. Arrays of Cherenkov telescope separated by 80-100 m provide geometric constraints on distance to Cherenkov event and direction of primary gamma-ray, thereby improving energy and angular resolution as well as eliminating background events due to local charge particles (muons).

3. VERITAS Design

The VERITAS TeV observatory[4] is a next generation gamma-ray instrument which simultaneously exploits the techniques of atmospheric Cherenkov imaging, geometrical array reconstruction, and fast readout electronics in order to realize substantial improvements in TeV gamma-ray sensitivity. The baseline VERITAS design is a distributed array of seven imaging air Cherenkov telescopes arranged in a hexagonal layout, with 80m spacing between the telescopes. The telescopes will be located at the base of Mt. Hopkins, south of Tucson, AZ. Figure 6 illustrates a typical array layout at a site that is currently under consideration for approval by the National Forest Service. The telescopes operate on dark, moonless nights, and can operate in independent mode, as a single, large sampling telescope array mode, or in a mixed mode with groups of three telescopes acting as a single instrument.

Independent (monocular) mode operation allows each telescope to track a different source in the sky, maximizing the celestial sky coverage. Array mode employs all seven telescopes to point to a single source in the sky, and triggers are formed by requiring coincident detection of the same gamma ray induced Cherenkov image by two or more telescopes. Array mode has the advantage that multiple telescopes image the shower from different observation points, providing stereo or tri-ocular geometrical event reconstruction. Multiple telescopes can also provide multiple measurements of primary energy, and therefore allow measurements of joint distributions of the reconstructed energy. These distributions can be used to directly estimate the energy resolution of a single telescope. The array mode coincidence requirement also allows energy threshold of the telescopes to be reduced over what is achievable with a single (monocular) telescope, thereby improving the detection aperture at low energies. Mixed mode consists of using some telescopes in an array mode with smaller numbers of telescopes in the arrays, an also some monocular (perhaps three telescopes observing one target and three observing another and a single monocular telescope observing a third source).

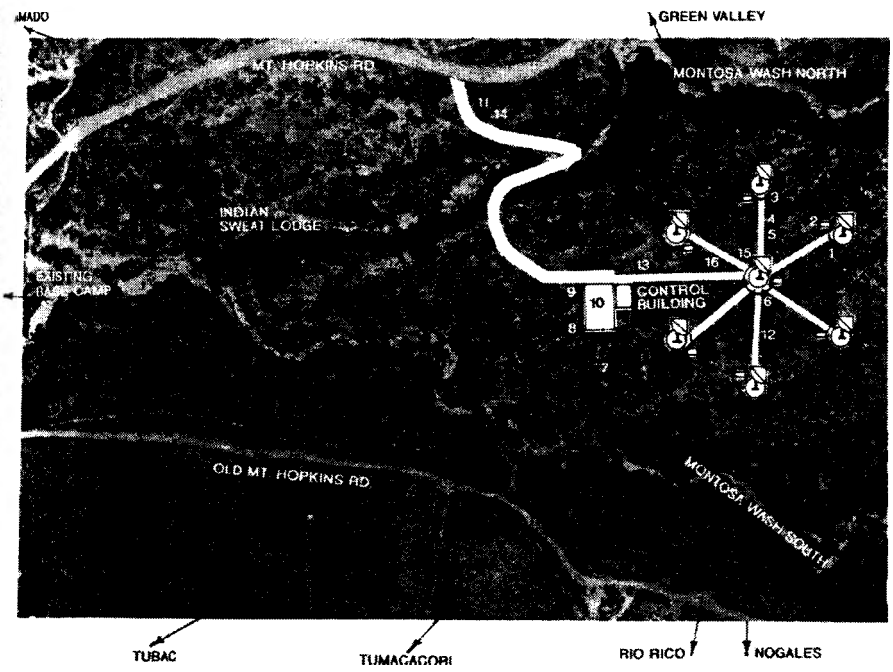

Figure 6: Overhead view of potential VERITAS observatory layout near Mt. Hopkins, AZ.

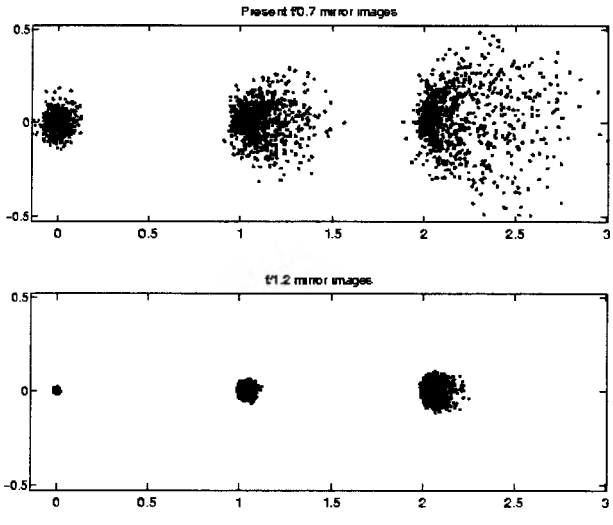

Figure 7:Images produced by a "Davies-Cotton" telescope 0°, 1°, and 2° from the optical axis for an *f*/0.7 telescope (upper panel) and an *f*/1.2 instrument (VERITAS). Both horizontal and vertical axes are in degrees.

3.1. Telescope Optical Design: Mirrors, Positioner, and Optical Support Structure

The desirable optical parameters of an atmospheric imaging Cherenkov telescope follow as a consequence of the characteristics of gamma-ray Cherenkov images. For an on-axis gamma-ray source the average image centroid is displaced ~0.85° from the optical axis. This value increases with increasing energy. The image has an r.m.s. width and length of about 0.14° and 0.25°. The reflector (telescope + camera) must have sufficient resolution to sufficient resolution to accurately record image structure on this scale.

In the VERITAS design, each telescope uses an f/1.2 10 m aperture Davies-Cotton reflector and an optical camera of 499 PMTs to view a 3.5 degree diameter of the night sky. The Davies-Cotton optical design[45] is composed of a segmented reflector in which the mirror facets of radius-of-curvature 2R are supported on a spherical optical support structure (OSS) surface of radius R. This design has smaller off axis aberrations than a parabolic reflector and the image quality is good out to a few degrees from the optical axis. Moreover, each mirror facet is spherical and identical, thereby simplifying fabrication and alignment. The facets are made of commercial float glass, heat slumped and polished, then aluminized and anodized. The 60 cm (edge-to-edge) mirror segments are hexagonal shaped to facilitate close packing.

The principle shortcoming of the Davies-Cotton is that it is not isochronous; an *f*/0.7 10 m reflector (the existing Whipple telescope) introduces a 6 nsec time spread to the Cherenkov light pulse. Increasing the *f*-number from *f*/0 to *f*/1.2 in the VERITAS design substantially improves the optical quality of the telescope (Figure 7) while decreasing the intrinsic time spread to ~ 4 nsec.

In order to maintain the desired image quality, the optical support structure must maintain mirror alignment to an angular accuracy of 0.01° throughout the range of operation. Effects gravity induced slumping of the image

at the face of the camera must be less than 2.2 mm at the face of the camera. Wind distortions should be less than 2 mm for wind speeds up to 30 m.p.h. Slew speed of > 1^0 per second on both axes is desirable for rapid retargeting to transient events. On the basis of a design study performed by an engineering firm, Simpson, Gumpertz and Heger (SG&H), it was determined that a custom designed square optical support structure of 10-12 m aperture and 12 m focal length mounted on a commercially available satellite/radio positioner (e.g. Antedo, Vertex-RSI, ViaSat, and RPM-PSI) could meet our design specifications for a wide range of operating conditions (Figure 8). The total weight of the OSS, mirrors, counterweight, and detector system is estimated to be 55,000 lbs.

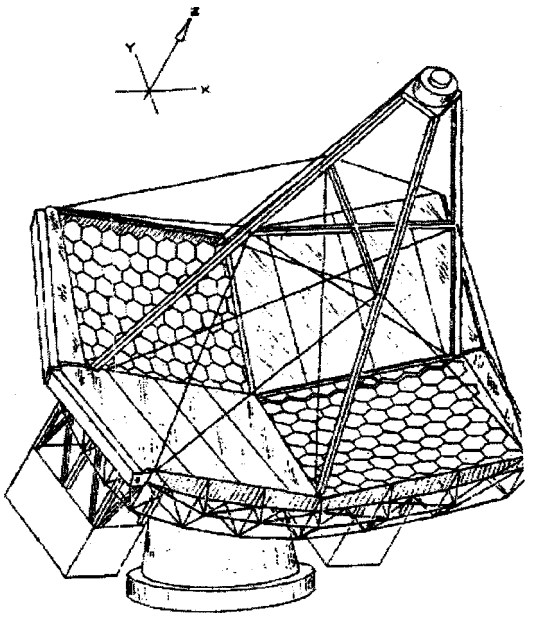

Figure 8: VERITAS telescope OSS and positioner design

3.2. Electronic Camera

Figure 9 provides a schematic overview of the components of a single telescope electronic camera. The focal plane detector consist of 499 hexagonally packed PMTs (Hamamatsu R1398-04) provide low noise, high gain (> 10^5) photon counting with risetime matched to the intrinsic time spread of photons in the gamma-ray induced Cherenkov image (2-3 nsec). The spacing of the PMTs corresponds to a focal plane angular distance of 0.15°. The active light collection diameter of the PMTs (25 mm) is increased by the use of Winston cone light concentrators. The PMTs are powered by a commercially available high voltage system (CAEN SY1527). The electronic signals from the PMTs are amplified in the camera and transmitted through 75Ω stranded-core RG-59 cable to local data recording electronics located at the telescope base.

3.3. Data Recording Electronics

Electronic signals from each pixel in the focal plane are split and sent to a 500 MHz Flash ADC (FADC) system of custom-built readout electronics and a separate trigger generation system that initiates data readout. Each FADC channel uses a commercially available 8-bit FADC chip with auto-ranging extending the dynamic range up to 10 bits. Each FADC chip continuously digitizes the electronic waveforms from each pixel into a circulating memory. When a readout trigger decision has been made by the trigger generation system, the associated electronics loads the appropriate section of FADC memory with relevant event information onto a high-speed data bus. The FADC information is then

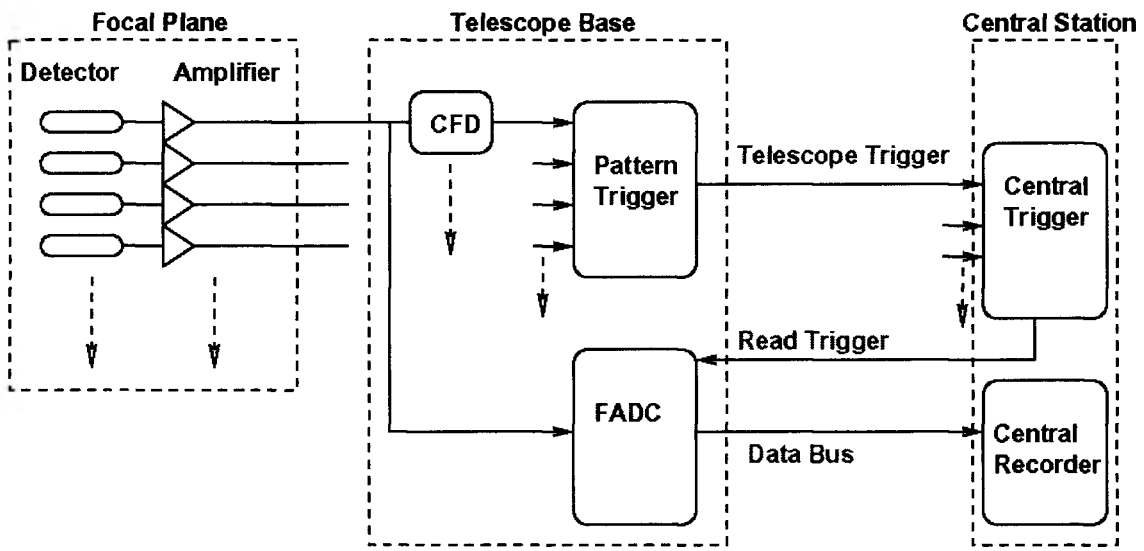

Figure 9: Schematic Outline of VERITAS Electronics

transmitted to the central station and recorded. A centrally generated pulse distributed by optical fibers is used to synchronize individual electronic channels and time tagging of events across the array.

The telescope electronics are based upon standard VME electronic architecture: a fast VME backplane for each FADC crate and distributed VME controllers connected by fiber optic data transport connections to a local telescope LINUX workstation. Each telescope workstation is connected via high-speed link to a central array processor that performs control, data compression and processing, and 'quicklook' data analysis to monitor array performance. The system operates using cyclic and multi-thread processes, adhering to POSIX standards where possible. For telescope readout rate of ~1 kHz each telescope is expected to have an average data flow rate of 800 Kbytes/s. This rate includes both real Cherenkov events as well as spurious background triggers.

In December 2001 a test of 30 channels of VERITAS front-end electronics was conducted at the Whipple telescope at Mt. Hopkins, AZ. This test included the entire signal chain, from PMTs to the FADC system. The PMTs were mounted on the edge of the existing Whipple telescope camera, and Cherenkov images were recorded using a simple majority logic trigger. Figure 10 illustrates a sample of an observed Cherenkov shower event. The recorded FADC waveform provides information about the signal pulse shape as well as a measurement of the noise level immediately before and after the Cherenkov light pulse.

3.4. *Triggering Scheme*

The combination of large mirror area, large pixel size, and operation in the open night sky generates a significant ambient background light level that determines the threshold for observation of Cherenkov light. For routine operation, the data recording electronics triggering rate is limited to trigger at a rate of < 1kHz. To facilitate this rate while keeping detector energy threshold to a minimum, a four-level triggering scheme has been devised. The levels are defined as:

Level 1:Pixel Trigger (CFD) Each Photomultiplier tube amplifier is fed into a constant fraction discriminator with programmable threshold. At low threshold, the dominant contribution to the background triggering rate is fluctuations in the night sky background. At higher thresholds (> 7 p.e.) the background triggering rate is dominated by PMT afterpulsing. Figure 11 illustrates the expected triggering rates in an individual pixel as a function of the pixel triggering threshold. For a typical pixel triggering threshold of 5.6 photoelectrons (p.e.), the expected triggering rate per pixel is approximately 500 kHz.

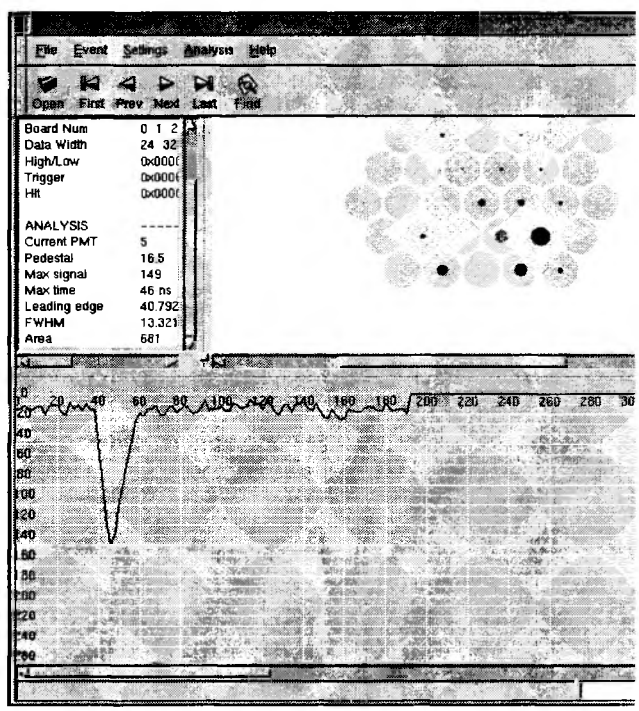

Figure 10: An example of a Cherenkov shower event collected during the 30 channel test. The upper right panel shows the assembly of tubes during the test with the diameter of the dark circles representing the signal amplitude. The lower panel shows a signal waveform recorded by the FADC electronics for a single pixel of this event. The time scale is in nsec.

Level 2: Telescope Pattern Trigger A hardware trigger, based upon digital trigger information from Level 1, is used to search for patterns of adjacent, simultaneously triggered pixels which are generated by Cherenkov images from gamma-rays. Pixel triggers generated by random fluctuations in the night sky background generally occur at random, non-adjacent pixel locations in the camera and therefore can be efficiently rejected. The dashed-dotted curve in Figure 11 shows the expected rate of these background events fulfilling a Level 2 pattern trigger requiring a minimum of 3 nearest neighbor pixels to be hit in the 499 pixel camera. At a threshold of 5.6 p.e, the Level 3 trigger rate is ~ 50 kHz per telescope.

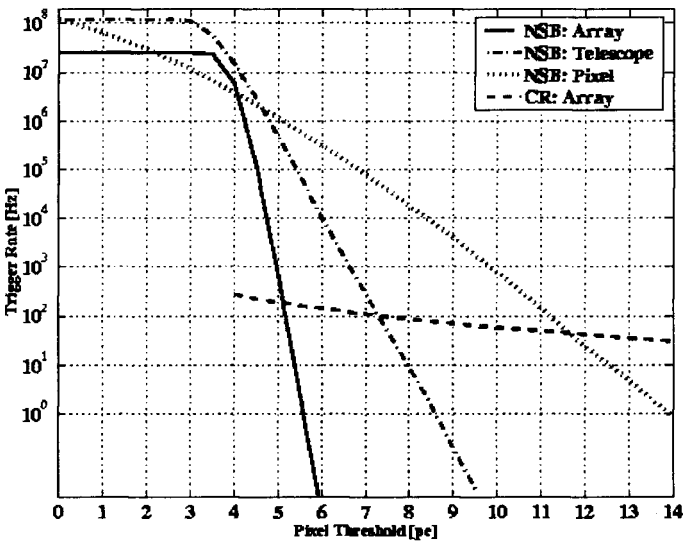

Figure 11: Expected background trigger rates for various trigger levels.

Level 3: Array Trigger By requiring multiple telescopes in the array to simultaneously observe the gamma-ray image, the background Level 2 trigger rate is further suppressed. A Level 3 array trigger is formed when 3 or 4 telescopes each produce a Level 2 pattern trigger within a coincidence time adjusted for arrival time delay of the Cherenkov light at each telescope. The solid curve in Figure 11 shows the expected background rates for the Level 3 trigger with 3 or 4 telescopes required within a 40 nsec coincidence window. At a threshold of 6 p.e. the array trigger produces negligible background rate trigger (less than a few Hz) from night sky fluctuations. The array trigger is dominated by real Cherenkov images generated by primary cosmic-rays and gamma-rays (dashed line in Figure 11).

Level 4: Reconstruction Trigger Although several telescopes are required to simultaneously observe an event within a narrow time window in order to generate a Level 3 trigger, there is no guarantee that these individual telescope events are consistent with a single gamma-ray/cosmic ray primary. By using the known physical location and pointing of each of the telescopes, one can ascertain whether the observed images in each telescope are simultaneously consistent with the expected parrallactic displacement and orientation for a single Cherenkov image. This system will further reduce the background trigger rate, and is currently under development using programmable delay hardware.

3.5. Calibration

In order to fully exploit the improved energy resolution of the array technique, VERITAS will employ several complementary calibration systems. Some of these systems include:

- Automated charge injection electronic calibration that can be used to diagnose and calibrate the data acquisition electronics during operation (at night) by day
- Automated optical injection from the central facility with similar light characteristics to Cherenkov light
- Measurement of atmospheric ground level aerosol scattering/absorption with fixed light sources at different elevations.
- Measurement of integrated atmospheric absorption by automated tracking of atmospheric extinction for transiting stars.

The VERITAS calibration system is designed as an integrated set of test that should prove channel-to-channel relative calibration to about 5% accuracy, and overall absolute energy calibration to approximately 12%.

4.Construction Timeline

Although VERITAS is envisaged as an array of seven telescopes, its modular design allows the construction to be divided into several distinct phases. The initial phase (which is currently underway) is the prototype phase, during which the first optical support structure, positioner, camera and associated electronics are designed, assembled, and tested in a working prototype system This phase began in mid-2001, and completion of the prototype phase is expected in mid-2003. Field testing of the prototype system on known steady-state gamma-ray sources (Crab nebula) will be used to assess the performance of single telescope (monocular) performance.

The first array phase of VERITAS (VERITAS: phase I) will deploy 4 telescopes, with the prototype telescope used as one of these 4 telescopes. VERITAS: phase I construction begins shortly after the evaluation of the single

prototype telescope in 2003, and is completed in 2005. After completion of the VERITAS: phase I array, the array system will be tested and qualified for routine operation. Subsequent to VERITAS: phase I, the three remaining VERITAS telescopes will be constructed to complete the full seven telescope array. It is expected that the final phase of VERITAS construction will take approximately 2 years, and would commence shortly after the commissioning of VERITAS: phase I.

5. Expected Performance

The expected scientific capabilities of the VERITAS array have been assessed via Monte Carlo simulation studies. In these studies, we have used the optical and electronic design characteristics described in Section 3. We assume a standard trigger criterion of requiring 3 adjacent pixels to record more than 5.6 p.e. per pixel in an 8 nsec coincidence window, and require a 3 telescope coincidence within a 40 nsec resolving time.

5.1. Angular reconstruction

We define the angular resolution as the half width of a 2-dimensional Gaussian fit to the central part of the distribution of reconstructed directions for individual gamma-rays from a point source. The angular resolution of VERITAS is a function of energy. The fraction of events that pass the trigger criteria and are reconstructed within a distance $\Delta\theta$ of the true source direction is shown in Figure 12 for three different photon energies. VERITAS will have a better angular resolution than any existing detector (in space or on the ground) above a few MeV. This capability is solely due to the stereoscopic geometrical reconstruction possible with the VERITAS array. The dramatic improvement in angular resolution will allow emission regions of extended sources to be mapped with arc minute accuracy.

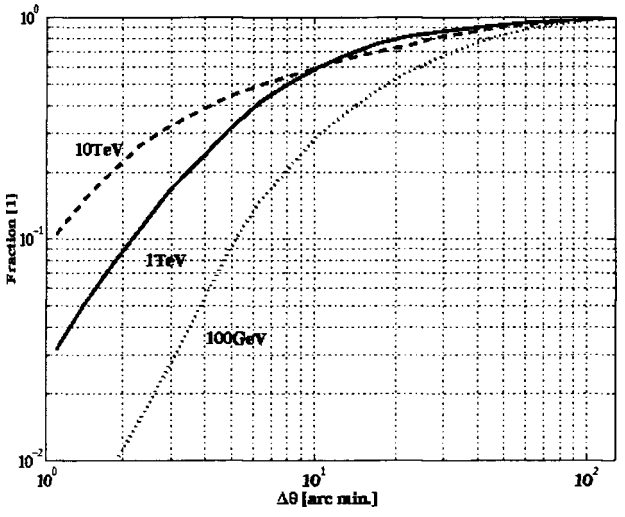

Figure 12: Fraction of triggering events whose arrival direction is reconstructed with error smaller than $\Delta\theta$ for three different gamma-ray energies.

5.2. Collection Area

The collection area of the array indicates its efficiency for triggering on gamma-ray showers. The collecting area of VERITAS as a function of photon energy is shown in Figure 13 for both VERITAS: phase I and the full VERITAS array. At high energies, the array will trigger on every incident shower, and the collection area saturates at the physical size of the detector (about 2×10^5 m^2).

5.3. Peak Energy

We define the peak energy of VERITAS as the energy at which the differential rate of detected gamma-rays from the Crab nebula per unit interval of energy reaches its maximum. The differential rate curves for VERITAS: phase I and the full VERITAS array, is shown in Figure 14. The falloff of the detected energy spectrum at high energies is due to the declining source spectrum, whereas the falloff at energies below 100 GeV is due to the rapid fall-off in detector collection area with decreasing energy in this region. The peak energy of ~100 GeV for both configurations is a factor 3 lower than that reached by existing imaging Cherenkov telescopes.

5.4. Point Source Sensitivity

Figure 15 compares the integral flux sensitivity of the full VERITAS array with the sensitivity of existing and upcoming space and ground-based telescopes. Integral flux sensitivities presuppose knowledge of the source spectrum and are not useful for sources with steep spectra that fall off near the energy threshold. However, many experiments present their sensitivities in this form and for comparison we have done the same for VERITAS[4]. In VERITAS:phase I the flux sensitivity will be close to that of the upper part of the shaded VERITAS line.

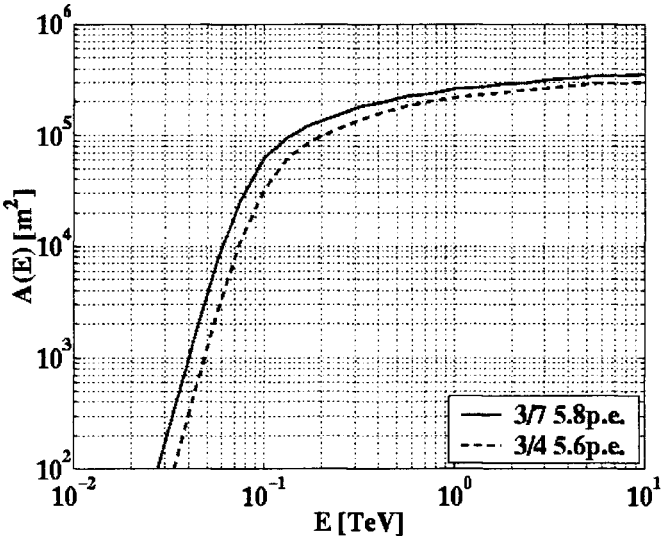

Figure 13: Collection area of VERITAS:phase I (dashed line) and full VERITAS Array (solid line) as a function of gamma-ray energy.

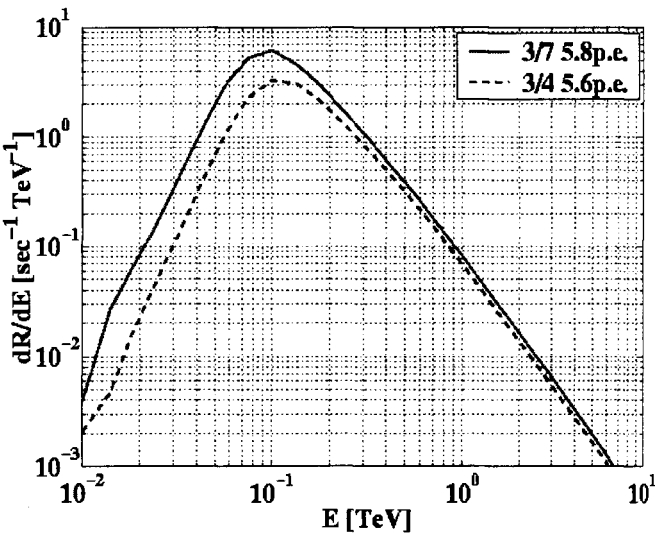

Figure 14: Differential Detection rates of the Crab Nebula for VERITAS:phase I (dashed line) and full VERITAS array (solid line).

It is apparent that on the low energy side, VERITAS will complement the GLAST satellite observatory[46], and will overlap with large ground based solar heliostat experiments (STACEE[47], CELESTE[48]). At higher energies VERITAS will overlap wide filed of view particle detectors (Milagro[49]and Tibet-AS[50]).

6. Summary

The VERITAS array is designed to be the world's most powerful generation ground-based TeV gamma ray observatory. VERITAS is being constructed by a collaboration of high-energy astrophysics groups at nine institutions. The VERITAS telescopes will achieve an order of magnitude better flux sensitivity than existing telescopes. It will be the only TeV gamma-ray telescope array in the northern hemisphere, and will therefore complement the southern hemisphere HESS [51]and CANGAROO[52] TeV observatories. As a northern hemisphere detector, VERITAS will also be in a unique position to observe potential neutrino sources discovered by AMANDA and ICECUBE at the South Pole[53].

7. Acknowledgements

The VERITAS Collaboration is supported by the U.S. Department of Energy, U.S. National Science Foundation, the Smithsonian Institution, P.P.A.R.C (UK) and Enterprise Ireland.

8. References

1. T.C. Weekes *et al., Ap. J.* **342**, 370 (1989).
2. G. Vacanti *et al., Ap. J.* **377**, 467 (1991).
3. T.C. Weekes, in *GeV-TeV Gamma Ray Astrophysics Workshop (Snowbird, Utah 1999)* AIP Conf. Proc **515**, 1 (2000).
4. T.C. Weekes *et al., Ap. Phys.* **17**, 221 (2002).
5. J. Quinn *et al., Ap. J.* **518**, 693 (1998).
6. J. Gaidos *et al., Nature* **383**, 319 (1996).
7. D.J. Macomb *et al., Ap. J.* **449**, L99 (1995).
8. J.H. Buckley *et al., Ap. J.* **472**, L9 (1996).

9. M. Catanese *et al., Ap. J.* **487**, L143 (1997).
10. K. Mannhein, *A&A* **269**, 67 (1993).
11. G. Ghisellini *et al., M.N.R.A.S.* **301**, 451 (1998).
12. M. Georganopoulos and A.P. Marscher, *Ap. J.* **506**, 621 (1998).
13. Costamante *et al., astro-ph/0112201* (2001).
14. J.H. Buckley, *Science* **279**, 676 (1998).
15. P.O. Lagage and C.J. Cesarsky, *A&A* **125**, 249 (1983).
16. M. Koyama *et al., Nature* **378**, 255 (1995).
17. F. Aharonian *et al., A&A* **370**, 112 (2001).
18. J.H. Buckley *et al., A&A* **329**, 639 (1998).
19. T. Kifune *et al., Ap. J.* **438**, L91 (1995).
20. T. Yoshikoshi *et al., Ap. J.* **487**, L65 (1997).
21. R.P. Gould and G.P. Schréder, *Phys. Rev.* **155**, 1408 (1967).
22. F.W. Stecker and O.C. de Jager, *A&A* **334**, L85 (1998).
23. E. Dwek and J. Slavin, *Ap. J.* **436**, 696 (1992).
24. S.D. Biller *et al.,Phys. Rev. Lett.* **80**, 2992 (1998).
25. V.V. Vassiliev, *Ap. Phys.* **11**, 247 (1999).
26. E. Waxman *et al.*, in preparation (2002).
27. S.W. Hawking, *M.N.R.A.S.* **152**, 75 (1971).
28. D.N. Page and S.W. Hawking, *Ap. J.* **206**, 1 (1976).
29. F. Halzen *et al., Nature* **353**, 807 (1991).
30. S. LeBohec, F. Krennrich, and T.C. Weekes, *Ap. J.* **539**, 209 (2000).
31. G. Amelino-Camelia *et al., Nature* **383**, 319 (1998).
32. E. Witten, *Nucl. Phys. B***471**, 135 (1996).
33. S.D. Biller *et al., Phys. Rev. Lett.* **83**, 2108 (1999).
34. L. Bergstrom, P. Ullio and J.H. Buckley, *Ap. Phys.* **9**, 137 (1998).
35. A. Tasitsiomi and A.V. Olinto, *astro-ph/0206040* (2002).
36. D.B. Kieda, S.P. Swordy, and S.P. Wakely, *Ap. Phys.* **15**, 287 (2001).
37. A. DeRujula, *Nucl. Phys. A***434**, 605 (1985).
38. J. Madsen, *hep-ph/0111417* (2001).
39. S.D. Wick *et al.*, submitted to *Ap. Phys. (astro-ph/0001233)* (2000).
40. T.C. Weekes and K.E. Turver, *Proc. 12th ESLAB Symp. (Frascati)* 279.
41. J.P. Finley *et al.*, in *GeV-TeV Gamma Ray Astrophysics Workshop (Snowbird, Utah 1999)* AIP **515**, 301 (2000).
42. F.A. Aharonian *et al., A&A* **342**, 69 (1999).
43. F.A. Aharonian *et al., A&A* **349**, 11 (1999).
44. A. Barrau *et al., Nucl. Inst. Meth.* **A416**, 278 (1998).
45. J.M. Davies and E.S. Cotton, *J. Solar Energy Sci. and Eng.* **1**, 16 (1957).
46. N. Gehrels and P. Michelson, in *TeV Astrophysics of Extragalactic Sources, Ap. Phys.* **11**, 277 (1999).
47. D.S. Hanna *et al. Nucl. Inst. Meth .A (in press) astro-ph/0205510* (2002).
48. B. Giebels *et al., Nucl. Inst. Meth A***412**, 329 (1998).
49. R. Atkins *et al., Proc. 27th Intl. Cosmic Ray Conf. (Hamburg, Germany)* (2001).
50. T. Yuda, *Proc. Intl. Symp. On Extremely High Energy Cosmic Rays (ICRR: Univ of Tokyo)* 175 (1996).
51. W. Hofmann , in *GeV-TeV Gamma Ray Astrophysics Workshop (Snowbird, Utah 1999)* AIP **515**, 500 (2000).
52. M. Mori *et al.*, ibid, 485 (2000).
53. J. Alvarex-Muniz and F. Halzen, *Proc. RADHEP-2000* , AIP **579**, 305 (2001).
54. E. Lorentz, in *GeV-TeV Gamma Ray Astrophysics Workshop (Snowbird, Utah 1999)* AIP **515**, 510 (2000).

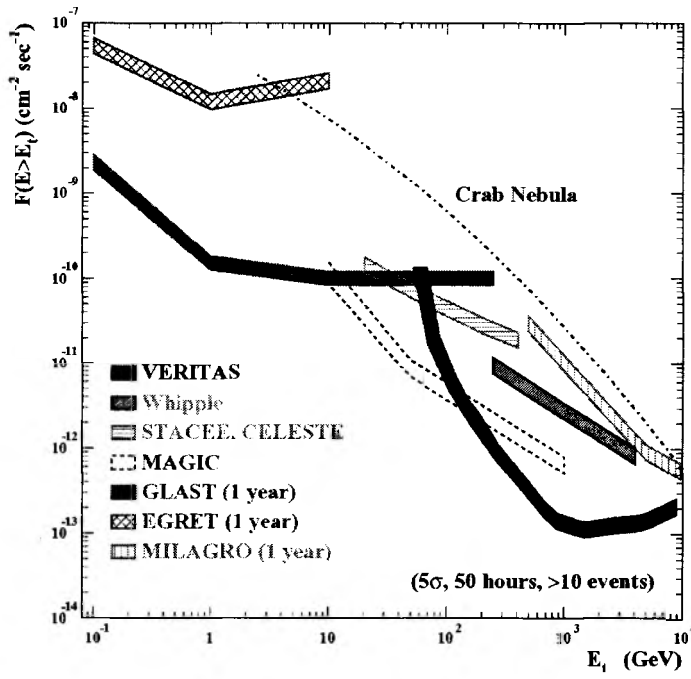

Figure 15: Comparison of point source sensitivity of VERITAS to Whipple, MAGIC[54], CELESTE/STACEE[47,48], GLAST[46], EGRET, and MILAGRO[49].